Mechanics Research Communications 53 (2013) 1–8

Contents lists available at ScienceDirect

Mechanics Research Communications

journal homepage: www.elsevier.com/locate/mechrescom

Elastoplastic damage modeling the mechanical behavior of rock-like materials considering confining pressure dependency

H. Zhou [a], H.B. Bian [b,c,*], Y. Jia [d], J.F. Shao [d]

[a] State Key Laboratory of Geomechanics and Geotechnical Engineering, Institute of Rock and Soil Mechanics, Chinese Academy of Sciences, 430071 Wuhan, China
[b] State Key Laboratory of Water Resources and Hydropower Engineering Science, Wuhan University, 430072 Wuhan, China
[c] LEM3, Université de Lorraine, ile du saulcy, 57000 Metz, France
[d] Lille Mechanics Laboratory, Polytech'Lille, Cité Scientifique, 59655 Villeneuve d'Ascq, France

ARTICLE INFO

Article history:
Received 13 October 2012
Received in revised form 1 April 2013
Accepted 15 July 2013
Available online 26 July 2013

Keywords:
Elasto-plasticity
Damage
Concrete
High confining pressure
Pore collapse

ABSTRACT

In this paper, the effect of confining pressure on the mechanical behavior of rock-like materials, such as concrete, is studied by using a coupled elastoplastic damage model. Damage mechanism is coupled, in different manners, with two plastic flow mechanisms: plastic shear mechanism developed under low confining pressure and plastic pore collapse mechanism observed under high confinement. The proposed model is applied to study a series of laboratory tests performed under extremely low to very high confining pressure, up to 650 MPa. The numerical predictions of proposed model are in good agreement with the experimental results.

1. Introduction

Rock-like materials, such as concrete, are widely used for making civil engineering structures, hydraulic buildings and nuclear power plants. In the terrorist or military conditions, these engineering structures may be subjected to the missile impact. As a result, the rock-like materials are subjected to a very high-intensity triaxial stress loading condition (Gran and Frew, 1997). The safety analysis of these structures requires modeling the effect of triaxial stress on mechanical behavior of construction materials. However, a majority of available research studies contribute to mechanical behavior of concrete under low and moderate triaxial stress loading conditions (Li and Pugh, 1970; Sfer et al., 2002). Recently, a series of triaxial compression tests have been performed on concrete with very high confining pressure, up to 650 MPa (Warren et al., 2004; Gabet et al., 2008; Vu et al., 2009; Malecot et al., 2010). These experimental investigations exhibit that the mechanical behavior of concrete depends strongly on applied confining pressure: a dramatic transition from brittle to ductile behavior is observed with the increase of confining pressure. Under low confining pressure, the failure process of concrete is characterized by important stiffness degradation induced by growth of micro-cracks and irreversible deformations. On the other hand, under high confining pressure, the degradation of material stiffness is significantly reduced and an important pore collapse phenomenon is observed. In particular, no failure stress is observed in stress–strain curves of triaxial compression tests under high confining pressure and the material exhibits ductile behavior. This phenomenon is due to the fact that the plastic pore collapse induces an increase of the contact surface between grains, which leads to a plastic hardening phase (Malecot et al., 2010). Consequently, it is necessary to formulate a constitutive model which is capable to describe the elastoplastic damage behavior developed under low to moderate confining pressure as well as the pore collapse hardening process observed under high confinement. In general, coupled elastoplastic damage models are used for the description of mechanical behavior of rock-like materials (Ju, 1989; Meschke et al., 1998; Contrafatto and Cuomo, 2006; Voyiadjis et al., 2008). Samani and Attard (2012) have given a brief review about constitutive models for concrete. However, these models focus essentially on the mechanical behavior of concrete under low to moderate confining pressure. In view of this, a new coupled elastoplastic damage model incorporating two plastic mechanisms (i.e., the plastic shear mechanism developed under low confining pressure and the plastic pore collapse mechanism observed under high confining pressure) will be proposed in present study. The emphasis is put on the plastic pore collapse process observed under high confining pressures.

* Corresponding author. Tel.: +33 387315258; fax: +33 387315366.
E-mail address: hanbing.bian@univ-lorraine.fr (H.B. Bian).

0093-6413/$ – see front matter © 2013 Elsevier Ltd. All rights reserved.
http://dx.doi.org/10.1016/j.mechrescom.2013.07.008

2. Coupled elastoplastic damage model for rock-like materials

In this section, an elastoplastic damage model is developed for rock-like materials. With the assumption of small strains, the total strain $d\underline{\underline{\varepsilon}}$ is decomposed into an elastic part $d\underline{\underline{\varepsilon}}^e$ and a plastic one $d\underline{\underline{\varepsilon}}^p$:

$$d\underline{\underline{\varepsilon}} = d\underline{\underline{\varepsilon}}^e + d\underline{\underline{\varepsilon}}^p, \quad d\underline{\underline{\varepsilon}}^p = d\underline{\underline{\varepsilon}}^{ps} + d\underline{\underline{\varepsilon}}^{pc} \tag{1}$$

Based on two plastic deformations observed at different confining pressure levels, the plastic deformation is divided into a shear part $d\underline{\underline{\varepsilon}}^{ps}$ corresponding to the plastic shear mechanism and a pore collapse one $d\underline{\underline{\varepsilon}}^{pc}$ relative to the plastic pore collapse mechanism.

For reason of simplicity, an isotropic damage is here adopted and represented by the scalar variable ω. Due to the different failure modes of rock-like materials under tension and compression conditions (i.e. cracking in tension and crushing in compression), the damage variable is decomposed in two parts: ω_c for the compressive damage and ω_t for the tensile one. Furthermore, the elastic modulus degradation is strongly dependent on micro-cracks: with open micro-cracks, the bulk and shear moduli are both affected by induced damage while the closed micro-cracks degrade only the shear modulus. In order to take into account such unilateral effects, the global damage variable ω is defined as following:

$$\omega = (1-\alpha_t)\omega_c + \alpha_t\omega_t \tag{2}$$

The coefficient α_t, which depends on the stress state, determines the different effects of tensile and compressive damage and is defined by the following function:

$$\alpha_t = \frac{\left\|\underline{\underline{\sigma}}^+\right\|}{\left\|\underline{\underline{\sigma}}\right\|} \tag{3}$$

$\underline{\underline{\sigma}}^+$ is the positive cone of stress tensor which can be obtained from the spectral decomposition based on the eigen values and vectors (Voyiadjis et al., 2008). For pure compressive stress state, one has $\alpha_t = 0$ while under pure tensile stress loading condition, $\alpha_t = 1$. The effective drained bulk and shear moduli of damaged material ($K(\omega)$, $G(\omega)$) are determined by following forms:

$$K(\omega) = K_0(1-\omega),\ G(\omega) = G_0(1-\omega) \tag{4}$$

K_0, G_0 are initial elastic properties of intact material.

In this study, the rock-like materials are assumed to be saturated by a liquid phase lq. The poroelastic behavior of saturated material will depend on the liquid pressure p_{lq}. Based on the previous work by Coussy et al. (1998), the elastic constitutive relations are expressed as:

$$d\underline{\underline{\sigma}} = \underline{\underline{\underline{\underline{C}}}}(\omega) : (d\underline{\underline{\varepsilon}} - d\underline{\underline{\varepsilon}}^p) + \frac{\partial \underline{\underline{\underline{\underline{C}}}}(\omega)}{\partial\omega} : (\underline{\underline{\varepsilon}} - \underline{\underline{\varepsilon}}^p)d\omega - \frac{\partial b(\omega)}{\partial\omega}p_{lq}d\omega\underline{\underline{\delta}} - b(\omega)dp_{lq}\underline{\underline{\delta}} \tag{5}$$

$\underline{\underline{\delta}}$ denotes the second order unit tensor. $b(\omega)$ denotes the Biot's coefficient and is determined by the following function:

$$b(\omega) = 1 - \frac{K(\omega)}{K_s} \tag{6}$$

K_s represents the compressibility modulus of solid matrix. The elastic stiffness tensor of damaged material $\underline{\underline{\underline{\underline{C}}}}(\omega)$ is written as the following form:

$$\underline{\underline{\underline{\underline{C}}}}(\omega) = 2G(\omega)\underline{\underline{\underline{\underline{K}}}} + 3K(\omega)\underline{\underline{\underline{\underline{J}}}} \tag{7}$$

Where isotropic symmetric fourth order tensors $\underline{\underline{\underline{\underline{K}}}}, \underline{\underline{\underline{\underline{J}}}}$ are defined by:

$$\underline{\underline{\underline{\underline{J}}}} = \frac{\underline{\underline{\delta}} \otimes \underline{\underline{\delta}}}{3}, \quad \underline{\underline{\underline{\underline{K}}}} = \underline{\underline{\underline{\underline{I}}}} - \underline{\underline{\underline{\underline{J}}}}, \quad I_{ijkl} = \frac{\delta_{ik}\delta_{jl} + \delta_{il}\delta_{jk}}{2} \tag{8}$$

$\underline{\underline{\underline{\underline{I}}}}$ is the symmetric fourth order unit tensor.

In the following sections, the basic components of plastic and damage mechanisms are presented in detail. Specific attention is paid to the pore collapse mechanism developed under high confinement. The formulation of damage is firstly presented.

2.1. Damage characterization

In the literature, a number of damage models have been proposed for rock-like materials in framework of irreversible thermodynamics. In these models, the damage evolution is determined by a damage criterion which is a function of thermodynamic forces associated with damage variables. However, in view of existing difficulties in mathematical determination of previous models, phenomenological models are generally used for modeling induced damage in studied material. In fact, the experimental investigations exhibit that in compressive regime, the material damage development is related to frictional sliding along micro-crack surfaces while in tensile regime, the damage evolution is inherently induced by tensile strains. In view of this, it is assumed that the damage variations, under tensile and compressive loading conditions, are respectively controlled by two different driving forces (Y^t_ω, Y^c_ω):

$$Y^t_\omega = \sqrt{\sum_{i=1}^{3}\langle\varepsilon_i\rangle^2} + \sqrt{\sum_{i=1}^{3}\left\langle\varepsilon_i + \frac{b_0}{3K_0}p_{lq}\right\rangle^2} \tag{9}$$

$$Y^c_\omega = \int\sqrt{\frac{2}{3}d\underline{\underline{e}} : d\underline{\underline{e}}}; \quad d\underline{\underline{e}} = d\underline{\underline{\varepsilon}} - \left(tr\frac{d\underline{\underline{\varepsilon}}}{3}\right)\underline{\underline{\delta}} \tag{10}$$

where $\varepsilon_i\,(i=1,3)$ denotes the three principal strain components. In Eq. (9), the first part $\sqrt{\sum_{i=1}^{3}\langle\varepsilon_i\rangle^2}$ is the sum of the positive total strain tensor. In order to take into account the influence of interstitial pressure, the second part $\sqrt{\sum_{i=1}^{3}\langle\varepsilon_i + (b/3K)p_{lq}\rangle^2}$ is introduced. b, K represent respectively the Biot's coefficient and the effective drained bulk of studied material. The bracket $\langle x\rangle$ means that only the positive value will be considered: $\langle x\rangle = 0$ if $x \le 0$ and $\langle x\rangle = x$ if $x > 0$.

Inspired by the damage model proposed by Mazars (1984), the evolutions of tensile damage and compressive damage are determined respectively by the following criteria:

$$f^t_\omega = \omega_t - \left(1 - \frac{1}{\exp(B_t Y^t_\omega)}\right) = 0 \tag{11}$$

$$f^c_\omega = \omega_c - \left(1 - \frac{1}{\exp(B_c Y^c_\omega)}\right) = 0 \tag{12}$$

The parameter B_c controls the kinetic of compressive damage and can be determined by using a uniaxial compression test. The parameter B_t characterizes the evolution of tensile damage and can be identified from a uniaxial tension test.

2.2. Plastic characterization

The plastic deformation of rock-like materials is controlled by the applied stresses as well as the liquid pressure. Therefore, the plastic functions should be one of all independent variables. However, these functions are very difficult to be experimentally

determined. One simplified approach, which consists in studying the saturated porous media by using relevant effective stress concept (Biot, 1956), is then adopted and extended in present study. The following effective stress tensor is introduced for plastic modeling of saturated concrete:

$$d\underline{\underline{\sigma}}^{pl} = d\underline{\underline{\sigma}} + \beta dp_{lq}\underline{\underline{\delta}} \tag{13}$$

The effective stress coefficient β controls the influence of liquid pressure on the plastic deformation. Aforementioned, under low and moderate confining pressures, the plastic shearing mechanism leads to the failure of rock-like materials by the formation of shear bands and crack coalescence. When the confining pressure exceeds a limit, the plastic deformation is controlled by the pore collapse process and material failure by shear bands/crack growth is not observed. In view of this, in the proposed model, the coupling processes between these two plastic deformations and damage are interpreted in different ways.

2.2.1. Plastic pore collapse characterization

Gurson (1977) proposed a plastic yield criterion which is capable to describe the pore collapse process in some porous media. Furthermore, this criterion has been largely used to describe the influence of porosity on plastic deformation in some rocks (Homand and Shao, 2000; Xie and Shao, 2006). Consequently, the following plastic yield criterion is used for modeling the pore collapse deformation:

$$f_c(\underline{\underline{\sigma}}^{pl}, \bar{\sigma}, \phi) = \frac{q^2}{\bar{\sigma}^2} + 2\phi\cosh\left[\frac{3p}{2\bar{\sigma}}\right] - 1 - \phi^2 = 0 \tag{14}$$

$$q = \sqrt{\tfrac{3}{2}\underline{\underline{s}}^{pl}\underline{\underline{s}}^{pl}}; \quad \underline{\underline{s}}^{pl} = \underline{\underline{\sigma}}^{pl} - p\underline{\underline{\delta}}; \quad p = tr\left(\frac{\underline{\underline{\sigma}}^{pl}}{3}\right) \tag{15}$$

q denotes the deviatoric effective stress while p is the mean effective stress. ϕ is the porosity of material. The coefficient $\bar{\sigma}$ represents the plastic yield stress of the solid matrix of studied material, which depends on the mechanical properties of solid grains and the various contact forces. Based on the experimental investigation from hydrostatic compression tests, a plastic isotropic hardening law is proposed as a function of plastic volumetric strain ε_M^{pc}:

$$\bar{\sigma} = \bar{\sigma}_0\left[1 + a(\varepsilon_M^{pc})^n e^{b\varepsilon_M^{pc}}\right], \quad \varepsilon_M^{pc} = tr(\underline{\underline{\varepsilon}}^{pc}) \tag{16}$$

In this function, $\bar{\sigma}_0$ defines the initial yield stress of solid matrix. a, b and n control the hardening law of pore collapse deformation. All these parameters can be determined from the volumetric strain versus applied hydrostatic stress curve in hydrostatic compression test. $\bar{\sigma}_0$ is obtained from the transition point form linear to nonlinear part. The three parameters a, b and n can be obtained by plotting plastic volumetric strain versus hydrostatic stress.

According to Eq. (14), the yield function of pore collapse process depends also on the connected porosity of material (see Fig. 1). By assuming that the plastic compressibility of solid grains may be neglected, the porosity change is expressed as following:

$$d\phi = (1-\phi)\varepsilon_M^{pc} \tag{17}$$

In order to describe satisfactorily the plastic volumetric deformation, a non-associated plastic flow rule is generally used for rock-like materials. By taking a similar form as the yield function, the following function is proposed as the plastic potential:

$$Q_c(\underline{\underline{\sigma}}^{pl}, \bar{\sigma}, \phi) = \frac{q^2}{\bar{\sigma}^2} + 2\phi\cosh\left(\frac{3p}{2\bar{\sigma}}\right) \tag{18}$$

2.2.2. Plastic shearing characterization

According to experimental data for concrete in various loading paths, under low to moderate confining pressure, the mechanical behavior of rock-like materials exhibits also a strong pressure dependency. Based on these experimental observations and inspired by the model proposed by Chen et al. (2007), the following equation is used:

$$f(\underline{\underline{\sigma}}^{pl}, \gamma^{ps}) = c_1\frac{q}{g(\theta)f_{c0}} + c_2\left(\frac{q}{g(\theta)f_{c0}}\right)^2 - \left(c_3 - \frac{p}{f_{c0}}\right) = 0 \tag{19}$$

The parameter f_{c0} represents the compression strength of rock-like materials, which can be identified from a uniaxial compression test. Three constants c_1, c_2, c_3 define the curvature of failure surface and can be determined by plotting the failure surface in the (p, q) plane (see Fig. 1). In the case $c_2 = 0$, the proposed model is equivalent to a Drucker–Prager type constitutive model, which is widely used in geomechanics. The function $g(\theta)$ defines the dependency of yield function on the Lode angle. In the absence of relevant data and for the sake of simplicity, the function $g(\theta)$ is taken as unity $g(\theta) = 1$. The yield criterion is defined in a similar functional form as Eq. (19):

$$f_s(\underline{\underline{\sigma}}^{pl}, \gamma^{ps}, \omega) = q - \alpha_s^{\omega}(\gamma^{ps})g(\theta)\bar{\sigma}_c = 0; \bar{\sigma}_c = \frac{\left(-c_1 + \sqrt{c_1^2 + 4c_2\left(c_3 - p/f_{c0}\right)}\right)}{2c_2}f_{c0} \tag{20}$$

In the proposed model, the post-peak softening phase is controlled by the damage evolution. Consequently, the rupture surface increases with the plastic distortion γ^{ps} and decreases with the damage evolution ω. Based on the experimental investigation, the following plastic hardening law is proposed:

$$\alpha_s^{\omega} = (1-\omega)\alpha_s, \quad \alpha_s = 1.0 - (1.0 - \alpha_s^0)e^{-B\gamma^{ps}}, \quad \gamma^{ps} = \int d\gamma^{ps} \tag{21}$$

$$d\gamma^{ps} = \int\sqrt{\frac{2}{3}d\underline{\underline{e}}^{ps} : d\underline{\underline{e}}^{ps}}, \; d\underline{\underline{e}}^{ps} = d\underline{\underline{\varepsilon}}^{ps} - \left(tr\left(\frac{d\underline{\underline{\varepsilon}}^{ps}}{3}\right)\right)\underline{\underline{\delta}}; \; \chi_p = \frac{\langle p - q/3 - p_r\rangle + p_r}{p_r} \tag{22}$$

The parameter B controls the kinetic of shear plastic hardening and can be obtained from the evolution of α_s versus plastic shear strain γ^{ps}. The function χ_p is introduced to better describe the strong pressure sensitivity of plastic hardening in studied material.

In order to suitably describe the plastic volumetric deformation developed under low to moderate confining pressure, a non-associated plastic flow rule should be adopted. Inspired by the previous work (Shao et al., 2006; Jia et al., 2010), the following plastic potential is used:

$$Q_s(\underline{\underline{\sigma}}^{pl}, \gamma^{ps}, \omega) = q + (1-\omega)\mu_s g(\theta) I\ln\left(\frac{I}{I_0}\right) = 0; \; I = -p + c_3 f_{c0} \tag{23}$$

The parameter I_0 defines the intersection of the plastic potential surface with the p axis. The boundary between compressibility and dilatancy domains is defined by the condition $\partial Q_s/\partial p = 0$, which is expressed as following:

$$f_{s\omega} = q - (1-\omega)\mu_s g(\theta)(-p + c_3 f_{c0}) = 0 \tag{24}$$

The parameter μ_s defines the slope of the boundary between compressibility and dilatancy domains. Its value can be obtained by plotting the transition boundary line in the p–q plane.

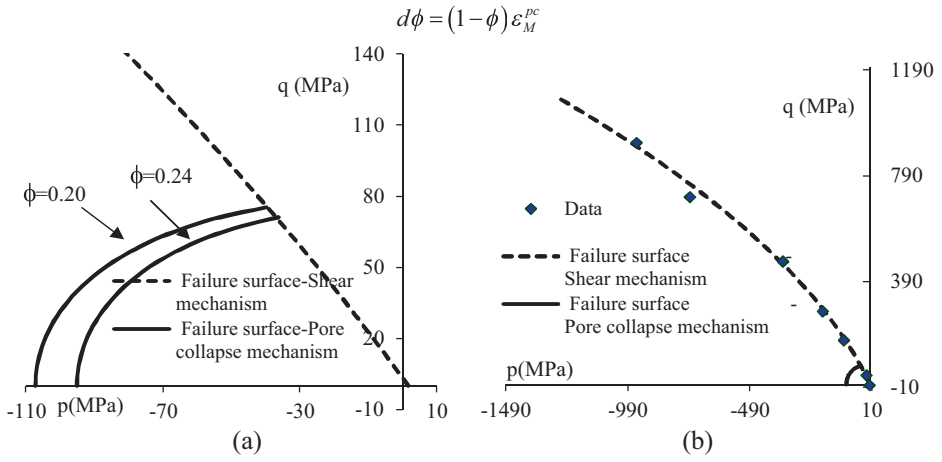

Fig. 1. Failure surface and pore collapse yield surface in p–q plane: (a) with different porosity values; (b) for studied materials.

3. The damage/plasticity coupling

In an elastoplastic damage model, plastic deformations and damage development generally occur in a coupled process. In view of this, the model's parameters are generally identified in three successive steps. Firstly, the plastic parameters are determined without the activation of damage mechanism. Using the obtained plastic parameters, the damage parameters are then identified. Finally, the plastic parameters will be adjusted in order to identify correctly the material failure. In order to avoid this adjustment of plastic parameters, a modified numerical damage variable ω^m is introduced and used in plastic functions.

3.1. Introduction of the modified numerical damage variable

In a coupled elastoplastic damage model, the material hardening is generally controlled by plastic strain while the material softening is dominated by damage. With the induction of modified numerical variable ω^m, one assumes that the plastic deformation is influenced by the damage evolution only in the softening phase. For instance, in a triaxial compression test, the effect of damage evolution on the plastic deformation will be taken into account after the peak stress.

When the material reaches its strength, the damage value of corresponding step will be saved as a reference value ω_0. The modified numerical damage value ω^m is then defined by the following function:

$$\omega^m = \frac{\langle \omega - \omega_0 \rangle}{1.0 - \omega_0} \tag{25}$$

The shear plastic yield function (20) and potential function (24) will be rewritten as following:

$$f_s(\underline{\underline{\sigma}}^{pl}, \gamma^{ps}, \omega^m) = q - (1-\omega^m)\alpha_s g(\theta)\bar{\sigma}_c = 0 \tag{26}$$

$$Q_s(\underline{\underline{\sigma}}^{pl}, \gamma^{ps}, \omega^m) = q + (1-\omega^m)\mu_s g(\theta) I \ln\left(\frac{I}{I_0}\right) = 0 \tag{27}$$

3.2. Interaction between damage and plastic behavior

In general, the damage mechanism and two plastic deformation mechanisms can be activated separately/simultaneously. According to the damage, a radial loading is assumed to determine the damage evolution rate with respect to two damage driving forces $d\alpha_t = 0$. As a result, the rate form of general damage variable can be given:

$$d\omega = \alpha_t d\omega_t + (1-\alpha_t) d\omega_c \tag{28}$$

According to the coupling of elasoplasticity and damage, four distinct domains can be identified during the general loading process:

1) If $f_c, f_s < 0$ and $d\omega > 0$: the applied stress state is fully inside the elastic domain. No plastic flow occurs while only damage evolution is observed. As a result, the increments of plastic strains are equal to zero: $d\underline{\underline{\varepsilon}}^{pc} = 0$, $d\underline{\underline{\varepsilon}}^{ps} = 0$ while the increment of damage $d\omega$ can be determined by the following function:

$$d\omega = (1-\alpha_t)\frac{B_c}{\exp(B_c Y_\omega^c)}\frac{\partial Y_\omega^c}{\partial \underline{\underline{\varepsilon}}} : d\underline{\underline{\varepsilon}} + \alpha_t \frac{B_t}{\exp(B_t Y_\omega^t)}\left(\frac{\partial Y_\omega^t}{\partial \underline{\underline{\varepsilon}}} : d\underline{\underline{\varepsilon}} + \frac{\partial Y_\omega^t}{\partial p_{lq}} dp_{lq}\right) \tag{29}$$

2) If $d\omega > 0$, $f_c = 0$ and $df_c = 0$ but $f_s < 0$, the damage mechanism and the plastic pore collapse mechanism are activated, while the plastic shear yield surface is not reached. In this case, we have $d\underline{\underline{\varepsilon}}^{ps} = 0$. As material failure by shear bands/crack growth is not observed in triaxial compression tests under high confining pressures, $d\omega$ and $d\underline{\underline{\varepsilon}}^{pc}$ should be identified separately. $d\omega$ can be obtained from the function (29) while the plastic pore collapse flow rule is written by:

$$d\underline{\underline{\varepsilon}}^{pc} = d\lambda_c \frac{\partial Q_c}{\partial \underline{\underline{\sigma}}^{pl}} \tag{30}$$

$$\frac{\partial Q_c}{\partial \underline{\underline{\sigma}}^{pl}} = \frac{\partial Q_c}{\partial q}\frac{\partial q}{\partial \underline{\underline{\sigma}}^{pl}} + \frac{\partial Q_c}{\partial p}\frac{\partial p}{\partial \underline{\underline{\sigma}}^{pl}} = \frac{3\underline{\underline{s}}}{\bar{\sigma}^2} + \frac{\phi}{\bar{\sigma}}\sinh\left(\frac{3p}{2\bar{\sigma}}\right)\underline{\underline{\delta}} \tag{31}$$

The plastic multiplier $d\lambda_c$ can be determined by the plastic consistency condition $df_c(\underline{\underline{\sigma}}^{pl}, \bar{\sigma}, \phi) = 0$:

$$d\lambda_c = \frac{\partial f_c/\partial \underline{\underline{\sigma}}^{pl} : \underline{\underline{\underline{\underline{C}}}}(\omega) : d\underline{\underline{\varepsilon}} + \beta\,\partial f_c/\partial \underline{\underline{\sigma}}^{pl} : dp_{lq}\underline{\underline{\delta}} + \partial f_c/\partial \underline{\underline{\sigma}}^{pl} : \partial \underline{\underline{\underline{\underline{C}}}}(\omega)/\partial\omega : \underline{\underline{\varepsilon}}^e d\omega}{\partial f_c/\partial \underline{\underline{\sigma}}^{pl} : \underline{\underline{\underline{\underline{C}}}}(\omega) : \partial Q_c/\partial \underline{\underline{\sigma}}^{pl} - \partial f_c/\partial\bar{\sigma}\,\partial\bar{\sigma}/\partial\varepsilon_M^{pc}\,\partial Q_c/\partial p - \partial f_c/\partial\phi(1-\phi)\,\partial Q_c/\partial p} \tag{32}$$

3) If $d\omega > 0$, $f_s = 0$ and $df_s = 0$ but $f_c < 0$, the damage mechanism and the plastic shear mechanism are activated while the plastic pore collapse surface is not reached. In this case, we have $d\underline{\underline{\varepsilon}}^{pc} = 0$. As the plastic shear mechanism is strongly coupled with damage, $d\omega$ and $d\underline{\underline{\varepsilon}}^{ps}$ should be determined simultaneously. $d\omega$ can be

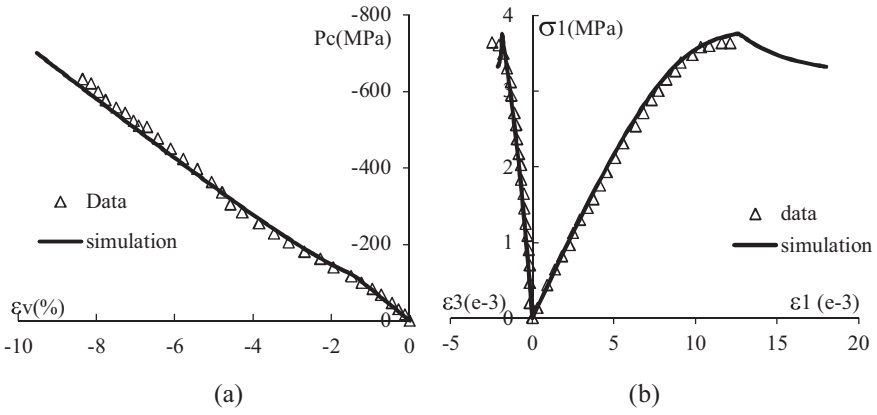

Fig. 2. Comparison between numerical prediction (continuous lines) and test data (points) in the case of (a) a hydrostatic compression test and; (b) a uniaxial tension test.

obtained from the function (29) while the plastic shear flow rule is written by:

$$d\underline{\underline{\varepsilon}}^{ps} = d\lambda_s \frac{\partial Q_s}{\partial \underline{\underline{\sigma}}^{pl}} \tag{33}$$

$$\frac{\partial Q_s}{\partial \underline{\underline{\sigma}}^{pl}} = \frac{\partial Q_s}{\partial q}\frac{\partial q}{\partial \underline{\underline{\sigma}}^{pl}} + \frac{\partial Q_s}{\partial p}\frac{\partial p}{\partial \underline{\underline{\sigma}}^{pl}} = \frac{3}{2}\frac{\underline{\underline{s}}}{q} + \frac{1}{3}\mu_s\left[1 + \left(\frac{I}{I_0}\right)\right]\underline{\underline{\delta}} \tag{34}$$

The plastic multiplier $d\lambda_s$ can be determined by the plastic consistency condition $df_s(\underline{\underline{\sigma}}^{pl}, \gamma^{ps}, \omega^m) = 0$:

$$d\lambda_s = \frac{\partial f_s/\partial \underline{\underline{\sigma}}^{pl} : \underline{\underline{\underline{\underline{C}}}}(\omega) : d\underline{\underline{\varepsilon}} + \beta\,\partial f_s/\partial \underline{\underline{\sigma}}^{pl} : dp_{lq}\underline{\underline{\delta}} + \left(\partial f_s/\partial \underline{\underline{\sigma}} : \partial \underline{\underline{\underline{\underline{C}}}}(\omega)/\partial\omega : \underline{\underline{\varepsilon}}^{e} + \partial f_s/\partial\alpha_s^{\omega}\,\partial\alpha_s^{\omega}/\partial\omega^m\,\partial\omega^m/\partial\omega\right)d\omega}{\partial f_s/\partial \underline{\underline{\sigma}}^{pl} : \underline{\underline{\underline{\underline{C}}}}(\omega) : \partial Q_s/\partial \underline{\underline{\sigma}}^{pl} - \partial f_s/\partial\alpha_s^{\omega}\,\partial\alpha_s^{\omega}/\partial\gamma^{ps}\,\partial\gamma^{ps}/\partial\underline{\underline{\varepsilon}}^{p} : \partial Q_s/\partial \underline{\underline{\sigma}}^{pl}} \tag{35}$$

4) If $d\omega > 0$, $f_s = 0$, $df_s = 0$ and $f_c = 0$, $df_c = 0$, both plastic flow and damage development occur. A nonlinear system of consistency conditions should be solved to determine the increments of plastic strains and damage:

$$\begin{cases} \left(\dfrac{\partial f_c}{\partial \underline{\underline{\sigma}}^{pl}} : \underline{\underline{\underline{\underline{C}}}}(\omega) : \dfrac{\partial Q_s}{\partial \underline{\underline{\sigma}}^{pl}} - H_{sc}\right)d\lambda_s + \left(\dfrac{\partial f_c}{\partial \underline{\underline{\sigma}}^{pl}} : \underline{\underline{\underline{\underline{C}}}}(\omega) : \dfrac{\partial Q_c}{\partial \underline{\underline{\sigma}}^{pl}} - H_{cc}\right)d\lambda_c - H_{c\omega}d\omega = F_c \\ \left(\dfrac{\partial f_s}{\partial \underline{\underline{\sigma}}^{pl}} : \underline{\underline{\underline{\underline{C}}}}(\omega) : \dfrac{\partial Q_s}{\partial \underline{\underline{\sigma}}^{pl}} - H_{ss}\right)d\lambda_s + \left(\dfrac{\partial f_s}{\partial \underline{\underline{\sigma}}^{pl}} : \underline{\underline{\underline{\underline{C}}}}(\omega) : \dfrac{\partial Q_c}{\partial \underline{\underline{\sigma}}^{pl}} - H_{cs}\right)d\lambda_c - H_{s\omega}d\omega = F_s \\ d\omega = (1-\alpha_t)\dfrac{B_c}{\exp(B_c Y_\omega^c)}\dfrac{\partial Y_\omega^c}{\partial \underline{\underline{\varepsilon}}} : d\underline{\underline{\varepsilon}} + \alpha_t\dfrac{B_t}{\exp(B_t Y_\omega^t)}\left(\dfrac{\partial Y_\omega^t}{\partial \underline{\underline{\varepsilon}}} : d\underline{\underline{\varepsilon}} + \dfrac{\partial Y_\omega^t}{\partial p_{lq}}dp_{lq}\right) \end{cases} \tag{36}$$

With $H_{ss} = \partial f_s/\partial\alpha_s^{\omega}\,\partial\alpha_s^{\omega}/\partial\gamma^{ps}\,\partial\gamma^{ps}/\partial\underline{\underline{\varepsilon}}^{ps} : \partial Q_s/\partial\underline{\underline{\sigma}}^{pl}$, $H_{cs} = 0$, $H_{sc} = 0$

$$H_{c\omega} = \frac{\partial f_c}{\partial \underline{\underline{\sigma}}^{pl}} : \frac{\partial \underline{\underline{\underline{\underline{C}}}}(\omega)}{\partial\omega} : \underline{\underline{\varepsilon}}^{e},\ H_{s\omega} = \frac{\partial f_s}{\partial \underline{\underline{\sigma}}^{pl}} : \frac{\partial \underline{\underline{\underline{\underline{C}}}}(\omega)}{\partial\omega} : \underline{\underline{\varepsilon}}^{e} + \frac{\partial f_s}{\partial\alpha_s^{\omega}}\frac{\partial\alpha_s^{\omega}}{\partial\omega^m}\frac{\partial\omega^m}{\partial\omega}$$

$$F_c = \frac{\partial f_c}{\partial \underline{\underline{\sigma}}^{pl}} : \underline{\underline{\underline{\underline{C}}}}(\omega) : d\underline{\underline{\varepsilon}} + \frac{\partial f_c}{\partial \underline{\underline{\sigma}}^{pl}} : \beta dp_{lq}\underline{\underline{\delta}},\ F_s = \frac{\partial f_s}{\partial \underline{\underline{\sigma}}^{pl}} : \underline{\underline{\underline{\underline{C}}}}(\omega) : d\underline{\underline{\varepsilon}} + \frac{\partial f_s}{\partial \underline{\underline{\sigma}}^{pl}} : \beta dp_{lq}\underline{\underline{\delta}}$$

In these equations, the two coefficients H_{cs}, H_{sc} represent the coupling effects between the hardening functions of two plastic mechanisms. In this study, one assumes that these two plastic mechanisms are independent. Consequently, in such a simplified case, we take $H_{cs} = H_{sc} = 0$. However, the general formulation of the proposed model is able to describe the hardening interaction between the two plastic mechanisms and the damage.

The proposed model is then implanted in a finite element code, called THMPASA, developed in the Lille Mechanics Laboratory. The numerical computation of proposed model is based on the classic step by step iterative method. It is composed of elastic prediction and plastic damage correction. At each step, a total strain increment is prescribed to each Gauss point of elements. The corresponding increments of stress, damage and plastic strains are identified by using the constitutive Eq. (5) and consistency conditions (29)–(36). With determined increments, the corresponding values of these variables are updated and the code goes back to the main block to verify the mechanical equilibrium.

4. Numerical simulation of laboratory tests

In this section, we take concrete (Gabet et al., 2008), one kind of rock-like materials, as an example to validate the proposed model. The parameters of proposed model can be identified by using a uniaxial tension test, a hydraulic compression test and a series of conventional triaxial compression tests performed under different levels of confining pressure. The input values for parameters of proposed model are summarized in Table 1.

Table 1
Representative values of model's parameters for concrete.

Parameters	Pore collapse plastic	Shear plastic	Damage
Values	$\bar{\sigma}_0 = -100$ MPa; $b = 200$ $a = 0.6$; $n = 0.12$	$c_1 = 0.5$; $c_2 = 0.02$; $c_3 = 0.05$ $f_{c0} = 33.5$ MPa; $B = 150$; $\mu_s = 1.5$	$B_t = 5$ $B_c = 10$

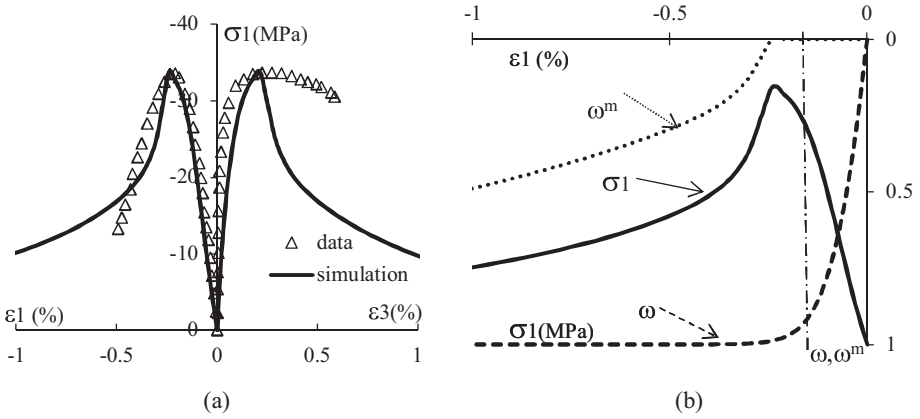

Fig. 3. Numerical simulation a uniaxial compression test: (a) comparison between numerical predications (continuous lines) and test data (points); (b) evolutions of ω, ω^m versus ε_1.

A hydrostatic compression test is firstly studied (Fig. 2a). Three phases can be identified from the curve of volumetric strain ε_v versus hydrostatic stress P_c. In the first phase, a quasi-linear and reversible stress–strain relation is observed when the confining pressure is less than 100 MPa. The mechanical behavior of concrete is essentially controlled by the porous and cohesive cement matrix. Consequently, the elastic bulk modulus can be determined directly by the slope of stress/strain curve. After that, when the hydrostatic stress reaches a limit value 100 MPa (i.e. the pore collapse yield stress), a sudden increase of irreversible plastic strain is produced. This phenomenon is relative to the plastic collapse process of pore structure. Finally, a plastic hardening phase, in which the volumetric strain rate increases, is clearly perceived at the end of hydrostatic compression test. This experimental observation can be explained by the fact that the pore collapse process induces a decrease in porosity and an increase of contact surface between grains. Generally, the plastic deformation due to the pore collapse process and the plastic hardening process created by the decrease of porosity can be satisfactorily described by the proposed model. A simple tension and a simple compression tests are then studied. The evolutions of axial stress σ_1 versus strain components (i.e. axial strain ε_1 and lateral strain ε_3) are presented in Figs. 2b and 3. The dissymmetric behavior of concrete under tension and compression conditions is satisfactorily captured by the proposed model. The evolutions of ω and ω^m in the uniaxial compression test are given in Fig. 3b. One observes that the variable ω^m, which controls the coupling between plasticity and damage, begins to increase as soon as the sample just softens. On the other hand, the elastic properties of studied material decrease progressively with the generalized damage variable ω from the beginning.

Furthermore, a series of triaxial compression tests performed under different confining pressures are simulated. Comparing different stress/strain curves, one observes that the mechanical behavior of concrete is dominated by plastic shear mechanism and damage mechanism under low to moderate confining pressure (50 and 100 MPa). Under the condition of zero confining pressure, a brittle failure is observed with an important softening regime in which the material failure occurs with a very small axial strain (see Fig. 3b). According to the tests realized under moderate confinements (Fig. 4), the stress/strain curves tend toward a plateau and a ductile failure is observed with a light softening phase. On the other hand, at high confining pressure levels (Fig. 5), the typical ductile failure is observed with an ultimate perfect plastic regime. Additionally, the axial strain corresponding to the failure state is very important. In general, one can observe that the mechanical behavior of concrete is significantly dependent on the applied confining pressure, including the increase of the concrete strength, the transition from brittle to ductile behavior and the material hardening processes created by the pore collapse mechanism. In conclusion, the general trend observed in experimental investigation is satisfactorily reproduced by numerical predictions.

As the previous experimental tests have been used for the determination of the model's parameters, these comparisons represent only a verification of the consistency of parameters. A lateral extension test and two proportional compression tests are then simulated in order to give a satisfactory validation of proposed model. The lateral extension test is given in Fig. 6. In this type of test, the sample is firstly subjected to a hydrostatic stress phase. The confining pressure (i.e. the lateral stress) is then decreased with a constant axial stress. A good agreement is obtained between experimental data and numerical simulations. Simulations of two

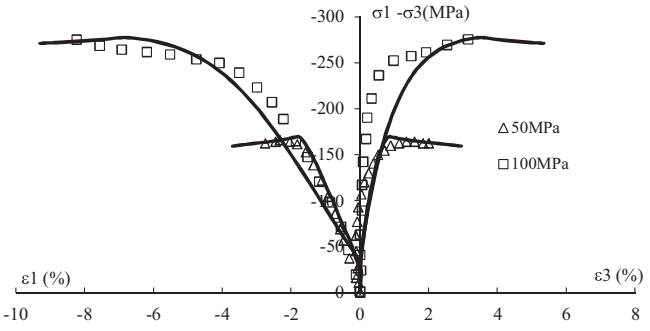

Fig. 4. Simulation of two triaxial compression tests under confining pressures 50 and 100 MPa.

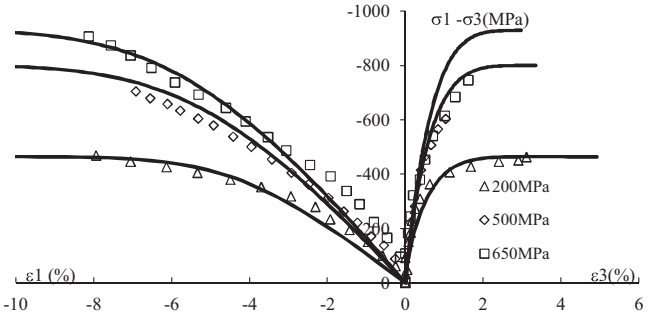

Fig. 5. Simulation of three triaxial compression tests under confining pressures 200, 500 and 650 MPa.

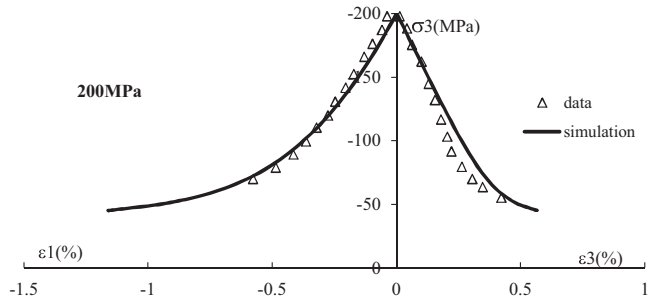

Fig. 6. Simulation of a lateral extension test with an initial confining pressure of 200 MPa.

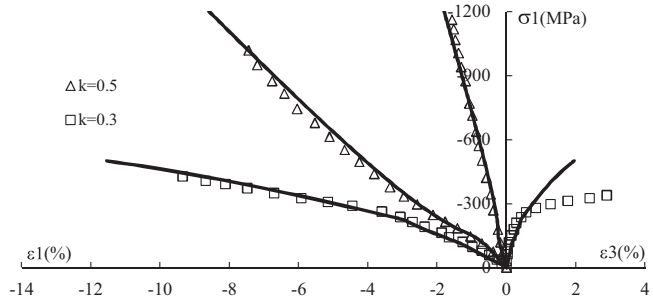

Fig. 7. Simulation of two proportional compression tests with the stress ratio $k = 0.3$ and 0.5.

proportional compression tests are presented in Fig. 7. In these tests, the axial stress σ_1 and lateral stress σ_3 are simultaneously increased with a constant ratio $k = \sigma_1/\sigma_3$. Again the simulations are in good concordance with test data. The comparisons between the numerical simulations and experimental data allow us to conclude that the proposed model is able to describe the mechanical behavior of concrete at a large range of applied pressure levels.

Finally, porosity variations in the deviatoric phases of triaxial compression tests are discussed. The curves of porosity ϕ versus $\varepsilon_1/\varepsilon_1^{peak}$ are presented in the Fig. 8a, where $\varepsilon_1/\varepsilon_1^{peak}$ denotes the ratio of the axial deformation to the value of axial strain at the peak stress level. At the beginning of deviatoric stress phase, the smallest value of porosity is obtained in the test performed under the confining pressure 650 MPa. This phenomenon is due to the fact that in the conventional triaxial compression test, the specimen is firstly loaded in a hydrostatic compression phase and then further loaded by increasing the axial load under constant confining pressure in the deviatroric phase. As a result, the studied material has been strongly compacted under the confining pressure 650 MPa. Comparison of different curves shows that in the uniaxial compression test, the porosity is constant. On the other hand, a decrease in porosity is generally observed with the increase of the deviatoric stress when the confining pressure exceeds 50 MPa. This observation is relative to the fact that when the applied stress is greater than the value of initial yield stress for pore collapse mechanism (i.e. 100 MPa), the pore collapse process is activated. Otherwise, the pores in the material will not be compacted. Moreover, the kinetic of porosity is analyzed by using the curves of $\varepsilon_1/\varepsilon_1^{peak}$ versus ϕ/ϕ_0^d (Fig. 8b), where ϕ/ϕ_0^d represents the ratio of actual value of porosity to the initial value of porosity at the beginning of the deviatoric phase. One observes that in the case where the applied confining pressure (50 MPa) is close to the initial yield stress for pore collapse mechanism, the pore collapse process is activated during tests and a decrease in porosity is then observed. In the case where the confining pressure (100 MPa, 200 MPa) exceeds the initial yield stress for pore collapse mechanism, the porosity of concrete decreases significantly. However, in the case where the confining pressures are very high (i.e. 500 MPa, 650 MPa), a slower decrease in porosity is observed. This phenomenon is due to the fact that the material has been strongly compacted in the hydrostatic phase and the initial yield stress of pore collapse increases with the decrease of porosity (Fig. 1a).

5. Conclusions

The mechanical behavior of the rock-like materials has been studied in this paper. A new coupled elastoplastic damage model is proposed for the studied material under a large range of confining pressure. Based on experimental investigation, two plastic deformation mechanisms and damage evolution have been taken into consideration: the plastic pore collapse mechanism developed under high confining pressure as well as the plastic shearing mechanism and induced damage observed under low and moderate confining pressures. In order to avoid the adjustment of plastic parameters in classic method, a modified numerical damage variable is introduced in the coupling of elastoplasticity and damage. The model's parameters can be determined from a hydrostatic compression test, a uniaxial tension test and a series of conventional triaxial compression tests. The simulations of laboratory tests, performed on various loading paths, have shown a good agreement with experimental data. In conclusion, the proposed model is able to describe the main features of poromechanical behavior for the rock-like material: dissymmetry in behavior under tension and compression conditions, important softening phase under low confining pressures and pore collapse process developed under high confining pressures. However, further advanced tests are still

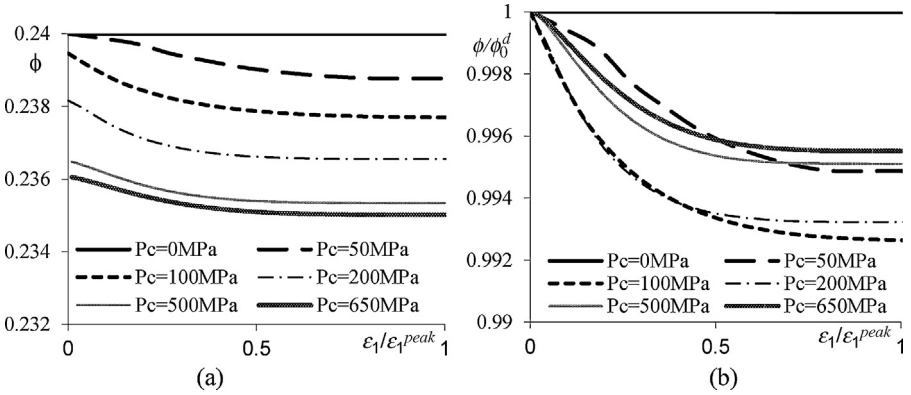

Fig. 8. Variation of porosity in deviatoric stress phase of triaxial compression tests under different confining pressures: (a) curves of $\varepsilon_1/\varepsilon_1^{peak}$ versus porosity ϕ; (b) curves of $\varepsilon_1/\varepsilon_1^{peak}$ versus ϕ/ϕ_0^d.

needed for an advanced validation of the proposed model, in particular under dynamic loading conditions. Some specific in situ experiments are also needed to verify the general validity of proposed model.

References

Biot, M.A., 1956. Theory of propagation of elastic waves propagation in a fluid saturated porous solid I. Low frequency Range. Journal of the Acoustical Society of America 28, 168–191.

Chen, D., Yurtdas, I., Burlion, N., Shao, J.F., 2007. Elastoplastic damage behavior of a mortar subjected to compression and desiccation. Journal of Engineering Mechanics 133 (4), 464–472.

Contrafatto, L., Cuomo, M., 2006. A framework of elastic–plastic damaging model for concrete under multiaxial stress states. International Journal of Plasticity 22, 2272–2300.

Coussy, O., Dormieux, L., Detournay, E., 1998. From mixture theory to Biot's approach for porous media. International Journal of Solids and Structures 35, 4619–4635.

Gabet, T., Malecot, Y., Daudeville, L., 2008. Triaxial behavior of concrete under high stresses: influence of the loading path on compaction and limit states. Cement and Concrete Research 38 (3), 403–412.

Gran, J.K., Frew, D.J., 1997. In-target radial stress measurements from penetration experiments into concrete by ogive-nose steel projectiles. International Journal of Impact Engineering 19 (8), 715–726.

Gurson, A.L., 1977. Continuum theory of ductile rupture by void nucleation and growth. Part I. Yield criterion and flow rules for porous ductile media. Journal of Engineering Materials and Technology 99, 2–15.

Homand, S., Shao, J.F., 2000. Mechanical behaviour of a porous chalk and water/chalk interaction. Part II: numerical modelling. Oil & Gas Science and Technology 55, 599–609.

Jia, Y., Bian, H.B., Su, K., Kondo, D., Shao, J.F., 2010. Elastoplastic damage modeling of desaturation and resaturation in argillites. International Journal for Numerical and Analytical Methods in Geomechanics 34 (2), 187–220.

Ju, J.W., 1989. On energy-based coupled elasto-plastic damage theories: constitutive modeling and computational aspects. International Journal of Solids and Structures 25, 803–833.

Li, H., Pugh, D., 1970. Mechanical Behavior of Materials Under Pressure. Elsevier, Amsterdam, pp. 1970.

Mazars, J., 1984. Application de la mécanique de l'endommagement au comportement non linéaire et à la rupture du béton de structure (in French). Université Paris 6, France (doctoral dissertation).

Malecot, Y., Daudeville, L., Dupray, F., Poinard, C., Buzaud, E., 2010. Strength and damage of concrete under high triaxial loading. European Journal of Environmental and Civil Engineering 14 (6–7), 777–803.

Meschke, G., Lackner, R., Mang, H.A., 1998. An anisotropic elastoplastic-damage model for plain concrete. International Journal for Numerical Methods in Engineering 42, 703–727.

Samani, A.K., Attard, M.M., 2012. A stress–strain mode for uniaxial and confined concrete under compression. Engineering Structure 41, 335–349.

Shao, J.F., Jia, Y., Kondo, D., Chiarelli, A.S., 2006. A coupled elastoplastic damage model for semi-brittle materials and extension to unsaturated conditions. Mechanics of Materials 38, 218–232.

Sfer, D., Carol, I., Gettu, R., Etse, G., 2002. Study of the behavior of concrete under triaxial compression. Journal of Engineering Mechanics 128 (2), 156–163.

Vu, X.H., Malecot, Y., Buzaud, E., Daudeville, L., 2009. Experimental analysis of concrete behavior under high confinement: effect of the saturation ratio. International Journal of Solids and Structures 46, 1105–1120.

Voyiadjis, G.Z., Taqieddin, Z.N., Kattan, P.I., 2008. Anisotropic damage-plasticity model for concrete. International Journal of Plasticity 24, 1946–1965.

Warren, T., Fossum, A., Frew, D., 2004. Experimental investigation of size effect in concrete fracture under multiaxial compression into low-strength (23 MPa) concrete: target characterization and simulations. International Journal of Impact Engineering 30, 477–503.

Xie, S.Y., Shao, J.F., 2006. Elastoplastic deformation of a porous rock and water interaction. International Journal of Plasticity 22, 2195–2225.